ADVANCED STUDY OF SWITCHABLE SPIN CROSSOVER COMPOUNDS
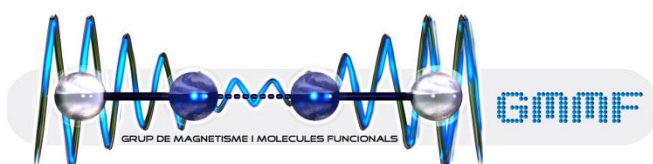
Universitat de Barcelona

Facultat de Química

Departament de Química Inorgànica

Programa de Doctorat: Química Inorgànica Molecular

Grup de Magnetisme i Molècules Funcionals

Gavin Craig

Director: Dr. Guillem Aromí Bedmar, Departament de Química Inorgànica

Tutor: Dr. Santiago Alvarez Reverter, Departament de Química Inorgànica

Advanced Study of
Switchable Spin Crossover Compounds

Gavin Craig

Contents

Chapter 4: Magneto-structural study of the compound [Fe(H₄L)₂](ClO₄)₂·H₂O·2(CH₃)₂CO

$$\text{[Fe(H}_4\text{L)}_2\text{](ClO}_4\text{)}_2\cdot\text{H}_2\text{O}\cdot2\text{(CH}_3\text{)}_2\text{CO}$$

4.0 Introduction

In Chapter 3, the spin crossover behaviour of a mononuclear Fe(II) compound involving the polypyrazolyl ligand 3-bpp was described. The spin transition appeared to be gradual and incomplete, signifying a low level of cooperativity. The development of the novel, polytopic ligand 2,6-bis(5-(2-hydroxyphenyl)-pyrazol-3-yl)pyridine (H₄L) (Figure 4.1) is geared towards improving the level of intermolecular interactions between the potentially spin-active cations, through the functionalisation of the bis-pyrazolyl core. In its uncoordinated form, the additional aromatic rings and hydrogen donor groups were shown to take an active part in the formation of the crystal lattice. The strategy therefore employed in this Chapter is again to coordinate the chelating species to Fe(II), with the intention that the extended nature of the ligand should favour a greater degree of communication between the metal sites.

These experiments led to the formation of the SCO compound [Fe(H₄L)₂](ClO₄)₂·H₂O·2(CH₃)₂CO (**1**), the molecular structure of which was confirmed by single crystal X-ray diffraction studies. The variable temperature magnetic behaviour of the system was investigated using SQUID magnetometry revealing a broad hysteresis loop, and the energetics associated with these transformations were derived from differential scanning calorimetry. The observation of a thermally trappable meta-stable HS state, both through magnetism and crystallography, shed light on the relationship between the spin transition and order/disorder phase transitions within the lattice.
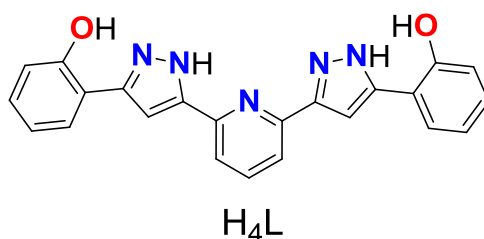
Figure 4.1: 2,6-bis(5-(2-hydroxyphenyl)-pyrazol-3-yl)pyridine (H₄L)

4.1 Synthesis

The synthesis of compound **1** followed the strategy employed for the majority of the compounds described in the thesis. Two molar equivalents of the ligand H_4L were reacted with one molar equivalent of $Fe(ClO_4)_2 \cdot H_2O$, in the presence of ascorbic acid, which acts as an anti-oxidant to prevent the formation of Fe(III) ions. Here, the solvent medium was acetone, and the orange solution produced on performing the reaction was layered with an equal volume of diethyl ether. After 7-10 days, this led to the formation of large polycrystalline aggregates of composition $[Fe(H_4L)_2](ClO_4)_2 \cdot H_2O \cdot 2CH_3COCH_3$ (**1**), as demonstrated by single crystal X-ray diffraction and confirmed by elemental analysis.

	Bond length/Å	
Bond	200 K	100 K
Fe-N3	2.133(2)	1.928(2)
Fe-N8	2.118(2)	1.930(2)
Fe-N2	2.171(2)	1.985(2)
Fe-N4	2.178(2)	1.992(2)
Fe-N7	2.206(2)	1.977(2)
Fe-N9	2.192(2)	1.981(2)
Average	2.166	1.966
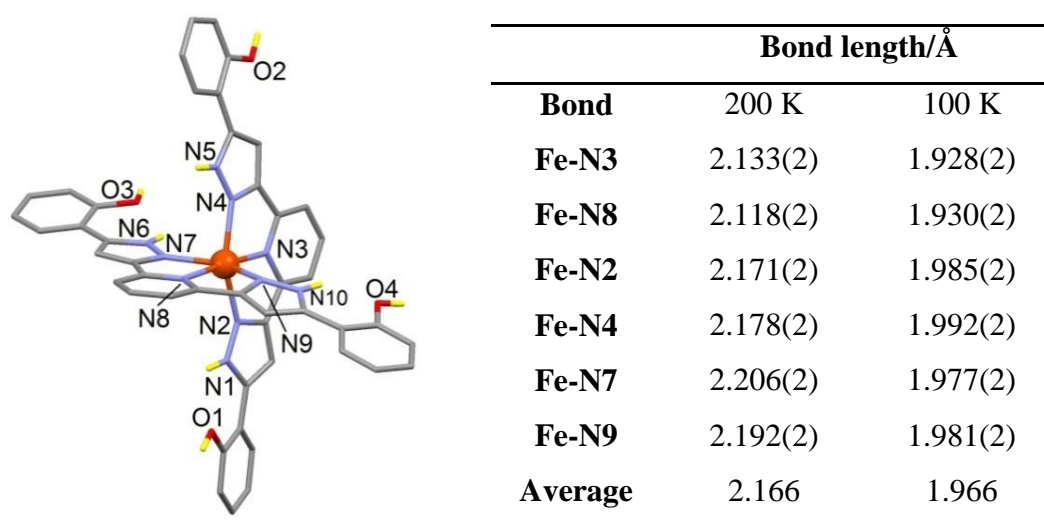
Figure 4.2 and Table 4.1: A Mercury view of the $[Fe(H_4L)_2]^{2+}$ cations in **1**. The hydrogen atoms are omitted for clarity, except those bonded to heteroatoms, shown in yellow. The six Fe-N bond lengths at 200 and 100 K are detailed in the table.

4.2 Single crystal X-ray diffraction study (I)

Breaking the polycrystalline aggregates of **1** yielded monocrystals suitable for single crystal X-ray diffraction studies. Resolution of the crystal structure at 200 and 100 K showed the compound to crystallise in the triclinic space group P_{-1}, with a unit cell that consists of the cation $[Fe(H_4L)_2]^{2+}$ (displayed in Figure 4.2), two ClO_4^- anions, two lattice molecules of acetone, and a lattice molecule of water. Full details of the structural refinement and selected structural parameters are given in Table 4.2. The complex cation is an Fe(II) ion with two neutral H_4L ligands coordinated through the three central nitrogen atoms of the pyridyl and pyrazolyl rings. To an approximation, the ligands lie

Compound	[Fe(H$_4$L)$_2$](ClO$_4$)$_2$·H$_2$O·2(CH$_3$)$_2$CO (1)				
T/K	200(HS)	150(HS)	150(LS)	100(LS)	100(Tr)
crystal system			Triclinic		
space group			P$_{-1}$		
a/Å	12.310(3)	12.275(3)	12.364(3)	12.326(3)	12.247(2)
b/Å	13.442(3)	13.407(3)	13.523(3)	13.513(3)	13.385(3)
c/Å	17.399(4)	17.386(4)	17.312(4)	17.269(4)	17.355(4)
α/°	104.57(3)	104.61(3)	106.69(3)	106.63(3)	104.60(3)
β/°	99.29(3)	99.25(3)	98.53(3)	98.50(3)	99.12(3)
γ/°	105.44(3)	105.39(3)	106.26(3)	106.36(3)	105.47(2)
V/Å^3	2604.1(13)	2588.7(13)	2578.0(13)	2560.5(13)	2574.4(12)
μ/mm^{-1}	0.520	0.522	0.524	0.528	0.525
Reflections collected	9823	9952	9955	9720	10009
*R*1 (all data)	0.0407	0.0506	0.0537	0.0495	0.0642
*wR*2 (all)	0.1178	0.1403	0.1555	0.1404	0.1779
S	1.064	1.071	1.044	1.020	1.035
av. Fe-N/Å	2.166	2.163	1.968	1.966	2.162
octahedral volume/Å^3	12.48	12.43	9.77	9.76	12.42
Σ/°	145.85	144.72	100.13	100.52	144.26
Φ/°	177.01	177.12	178.62	178.53	177.05
θ/°	74.94	74.90	77.54	77.17	74.66
Θ/°	469.18	466.03	310.82	311.17	464.04

Table 4.2: Crystallographic data and selected structural parameters for compound **1**.

each in their own plane, and the bite angle of the polypyrazolyl ligand means that the FeN$_6$ coordination sphere is a distorted octahedron. The average Fe-N bond length is 2.166/1.966 Å (200/100 K) which correspond to an Fe(II) centre in the HS and LS states, respectively (see Table 4.1).[1] The dihedral angle θ that is formed by the ligand's disposition in two different planes measures 74.94/77.17°, and the N3-Fe-N8 angle Φ is 177.01(2)/178.53(2)°; demonstrative of an increased regularity of the shape of the molecule in the low spin state, which displays values closer to the ideal of values of 90° and 180°, respectively.[2] The parameters Σ and Θ, which are used as a means of measuring

the distortion of the coordination octahedron away from O_h symmetry towards D_{3h} symmetry,[3, 4] are 145.85/100.52° and 469.18/311.17°, indicating that the HS state is associated with a more highly distorted coordination octahedron. The extended aromatic wings of the ligand H_4L show two different conformations with respect to the central Fe(II) ion, with one ligand displaying a *syn,syn* arrangement of the phenol rings, while the other ligand is *syn,anti*. These aromatic wings and hydrogen donor groups give rise to the array of intermolecular interactions that mediate the contact between the $[Fe(H_4L)_2]^{2+}$ cations and hold the lattice together.
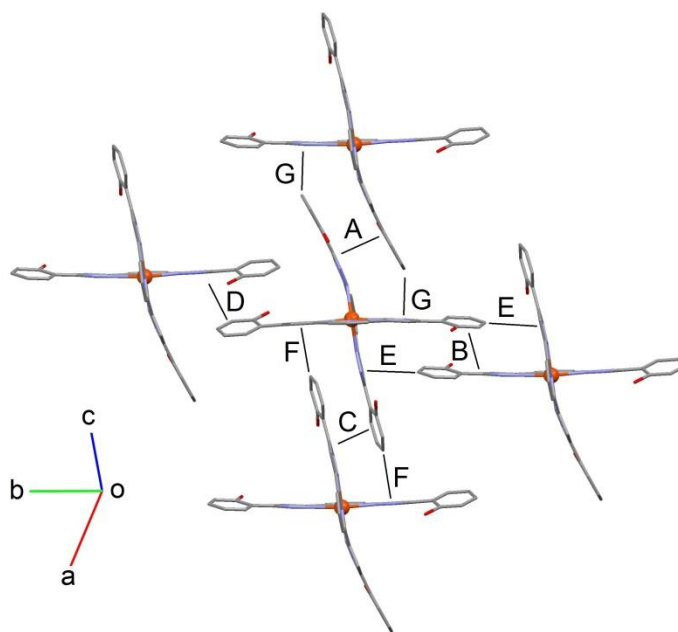
Contact	Labels	Distance/Å	
$\pi\cdots\pi$		200 K	100 K
A	pz···phen	3.598(2)	3.547(2)
B	pz···phen	4.733(2)	4.448(2)
C	pz···phen	4.113(2)	3.767(2)
D	pz···phen	4.465(2)	4.251(2)
C-H···π			
E	C21-H21A···pz	3.722(3)	-
F	C26-H26A···pz	3.412(3)	3.336(3)
G	C43-H43A···pz	-	3.691(3)

Figure 4.3 and Table 4.3: A representation of the co-planarity induced in **1** by $\pi\cdots\pi$ and C-H···π interactions, hydrogen atoms omitted for clarity. The table shows the distances for each contact at 200 and 100 K, between centroids defined by the program PLATON.[7] pz = pyrazolyl ring and phen = phenol ring.

The shape of the complex cation favours the formation of a crystal packing arrangement analogous to the so-called terpyridine embrace,[5, 6] where the faces of the aromatic wings come within sufficient proximity of each other to allow overlap, and these interactions are then reinforced by C-H$\cdots\pi$ contacts, where the C-H bond on the edge of an aromatic ring interacts with the face of an adjacent aromatic ring (Figure 4.3). The distal rings of the ligand can therefore take part in four such $\pi\cdots\pi$ interactions, where the phenol ring of one cation lies close to the pyrazolyl ring of the adjacent cation, and vice-versa. The average strength of these interactions, reflected by the average distance between the aromatic rings, at 200 K is 4.227 Å, and the transition to the LS state sees a reinforcement reflected by a decrease in this value to 4.003 Å (Table 4.3). The $\pi\cdots\pi$ overlaps are then complemented by C-H$\cdots\pi$ contacts, which illustrate the dynamic nature of the structure on lowering the temperature. The average strength of this latter class of interactions increases (3.567/3.514 Å), and this is accompanied by the rupture of one of the two interactions observed at 200 K (C21-H21A$\cdots$pz; **E**), and the formation of a new interaction at 100 K (C43-H43A$\cdots$pz; **G**). The combination of these $\pi\cdots\pi$ overlaps and C-H$\cdots\pi$ contacts brings the cations together in planar 2D networks, which are then connected through hydrogen bonding motifs in which the cations, anions, and lattice solvents participate.

The interaction between layers is thus largely conducted through the wings of the H_4L ligand (see Figure 4.4). There are two differing ways in which this can occur; in the first, the *syn,syn* ligand on one side links through the external phenol ring (O3) to a perchlorate anion (O8), which in turn interacts with the phenol (O4), pyrazolyl (N10), and pyridyl rings (**B**) of the cation in the next layer. The inverse of this arrangement occurs on the other side of the *syn,syn* ligand through crystal symmetry. In the second, between the *syn,anti* ligands, a pyrazolyl ring (N5) forms a hydrogen bond with a perchlorate (O9), which then interacts with the distal phenol ring of the adjacent cation through O1. This phenol ring, together with the adjoining pyrazolyl group, displays an interaction with the lattice molecule of water. The exact effect on the spin state of the Fe(II) centre of the H_2O molecule hydrogen bonding to the pyrazolyl ring is unclear, in the literature it has been proposed that this increases the basicity of the ligand, and stabilises the LS state.[8] In both of these arrangements, the disposition and proximity of the pyridyl rings allow a face-to-face interaction (**A** and **C**) the average strength of which increases on lowering the temperature.
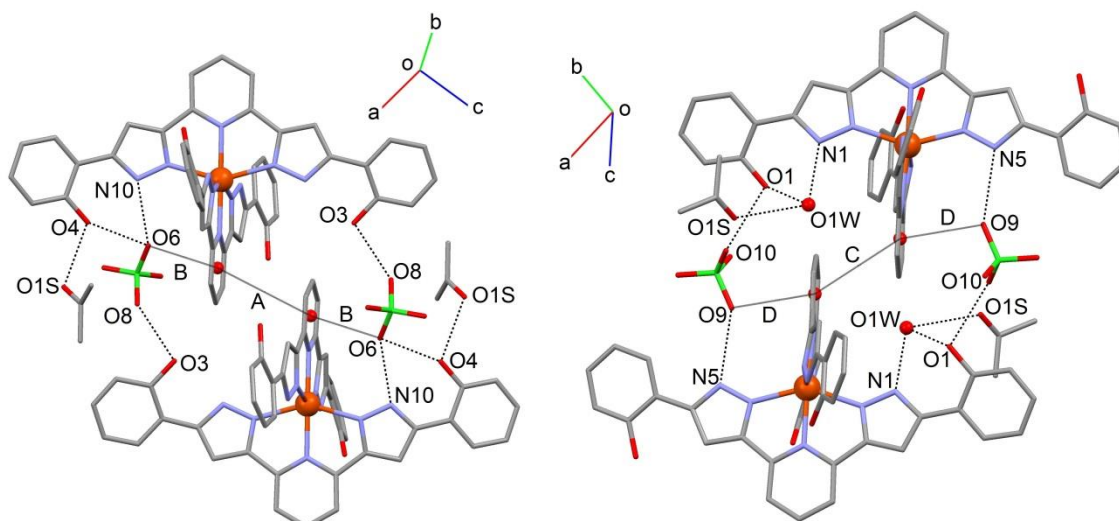
Contact	Distance/Å	
(left)	200 K	100 K
O3-H3···O8	2.747(3)	2.908(3)
O4-H4···O1S	2.769(3)	2.767(3)
O4-H4···O6	2.993(2)	3.168(3)
N10-H10···O6	2.934(3)	2.834(3)
A = Cg9(py)···Cg9(py)	4.802(2)	4.730(2)
B = O6···Cg9(py)	3.412(3)	-
Fe···Fe	9.742(3)	9.833(2)
(right)		
N1-H1···O1W	2.862(2)	2.937(3)
N5-H5···O9	2.893(2)	2.938(3)
O1-H10···O10	2.876(3)	2.818(3)
O1-H1···O1W	2.979(2)	2.946(3)
O1W···O1S	2.904(3)	2.993(3)
C = Cg10(py)···Cg10(py)	4.566(2)	4.607(2)
D = O9···Cg10(py)	3.178(2)	3.236(2)
Fe···Fe	9.908(2)	9.854(3)

Figure 4.4 and Table 4.4: The hydrogen bonding motifs and metric parameters for the interactions that exist between the 2D layers in **1**, with hydrogen atoms omitted for clarity.

4.3 Magnetic properties (I)

The magnetic properties of a polycrystalline sample of compound **1** were measured in the 5-300 K temperature range under a magnetic field of 5 kG (Figure 4.5). At high temperatures, the molar magnetic susceptibility product given by χT measures 3.46 cm^{3}mol^{-1}K, which is consistent with an Fe(II) ion in the HS state ($S = 2$, $\chi T = 3.0$ cm^{3}mol^{-1}K, for $g = 2$),[9] and with the 200 K crystal structure. On lowering the temperature at a rate of 1 Kmin^{-1}, χT remains almost constant, as the compound stays in the HS state. At 150 K, the magnetic response of the compound begins to decrease, as the HS paramagnetic Fe(II) ions begin to switch to the LS diamagnetic state. This process continues until 90 K, where $\chi T = 0.15$ cm^{3}mol^{-1}K, which corresponds to a residual fraction of Fe(II) in the HS state of 4 %, and this value remains constant to the lowest temperatures measured. This spin crossover on cooling is associated with a value of $T_{1/2}(\downarrow) = 133$ K. In the heating mode, the χT curve re-traces that measured on cooling, until 90 K, where the magnetic response diverges from that of the cooling mode. The system remains in a LS state until 170 K, where an abrupt transition occurs, returning all of the Fe(II) ions to the HS state at 175 K ($T_{1/2}(\uparrow) = 173$ K). Therefore, compound **1** shows a complete thermal SCO, with a broad hysteresis loop of ~40 K. The asymmetric nature of the observed hysteresis loop suggests that the dynamics of the HS→LS must differ from the significantly sharper LS→ transition.
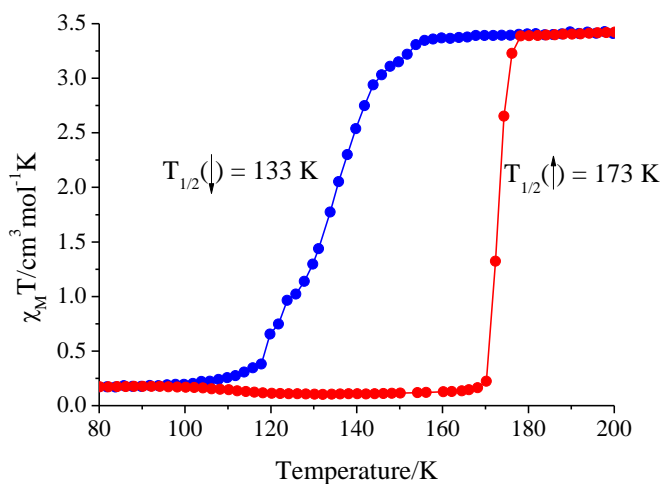

Figure 4.5: The molar magnetic susceptibility product, χT *vs*. the temperature, T, for a polycrystalline sample of **1** in the temperature range 200 to 80 K, measured at a rate of 1 Kmin^{-1}. The cooling mode is shown in blue, and the heating mode is shown in red.

The robustness of the hysteresis loop for a polycrystalline sample of **1** was demonstrated by performing various thermal cycles in the SQUID magnetometer together with DSC measurements (Figure 4.6). Over four cycles, the temperature range over which the compound is bi-stable was not found to vary, and the LS→HS transition was observed at the same temperature in the heating branch, and to be of the same energetics (see Section 4.4 for a more detailed explanation of DSC measurements). The slight difference in the cooling branch is attributed to the cooling rate used, which was 0.7 Kmin^{-1}. The durability of this bi-stable region is associated only with compound **1** in the polycrystalline or single crystal forms. Grinding of the sample to a fine powder results in the magnetic behaviour shown in Figure 4.6. Here, the system remains in the HS over the entire range of temperatures on variation at 1 Kmin^{-1}. The value of χT at 200 K is 3.21 cm^{3}mol^{-1}K, and on lowering the temperature the magnetic response is nearly constant, until zero field splitting effects[10] below 20 K reduce χT to 1.92 cm^{3}mol^{-1}K at 2 K. This severe modification of the magnetic properties displayed is attributed to the impact that grinding a sample has on the extensive network on intermolecular interactions which holds **1** together within the lattice.[11]
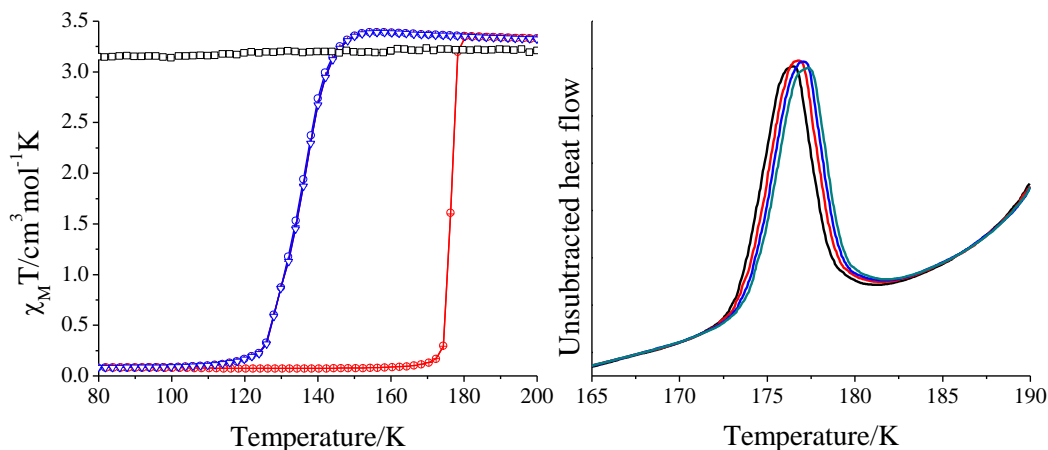
Figure 4.6: (left) 3 thermal cycles conducted on a polycrystalline sample of **1** in blue (cooling mode) and red (heating mode). The black squares represent the χT product for **1** in the powder form. (right) The unsubtracted heat flow associated with the LS→HS transition observed on cycling **1** four times.

4.4 Differential Scanning Calorimetry (DSC)

The thermal properties of a polycrystalline sample could be investigated using differential scanning calorimetry (DSC), in both the cooling and heating modes. The data are

represented in Figure 4.7 as the raw heat flow data *vs.* temperature, where the less abrupt nature of the HS➔LS transition can be observed as a very broad hump in the range 150 – 120 K. This is in contrast to the trace obtained in the heating mode where a sharp peak at 172 K corresponds to the LS➔HS transition. The distinct appearance of the traces is consistent with the asymmetric hysteresis loop observed in the SQUID magnetometer. Subtraction from the heat capacity measurement, C_P, of a lattice heat capacity curve, C_{lat}, estimated from the data at high and low temperatures on either side of the anomalies, yields the excess heat capacity, ΔC_P (Figure 4.7).[12] Integration of this quantity over $ln(T)$ and T, leads to the values of the excess entropy, ΔS, and excess enthalpy, ΔH, associated with the transition, respectively. For compound **1**, the transition to the singlet state gives $\Delta S = 26.7$ Jmol^{-1}K^{-1} and $\Delta H = 3.53$ kJmol^{-1}, while the return to the quintet state gives $\Delta S = 54.1$ Jmol^{-1}K^{-1} and $\Delta H = 9.29$ kJmol^{-1}. These values of excess entropy exceed the expected value for a change purely of the spin state (Rln(5) $= 13.4$ Jmol^{-1}K^{-1}), which indicates a vibrational component to the parameter, due to both the intramolecular vibrational modfications and to intermolecular interactions found within the crystal lattice of **1**. They also reflect the more cooperative nature of the LS➔HS transition with respect to the inverse process.
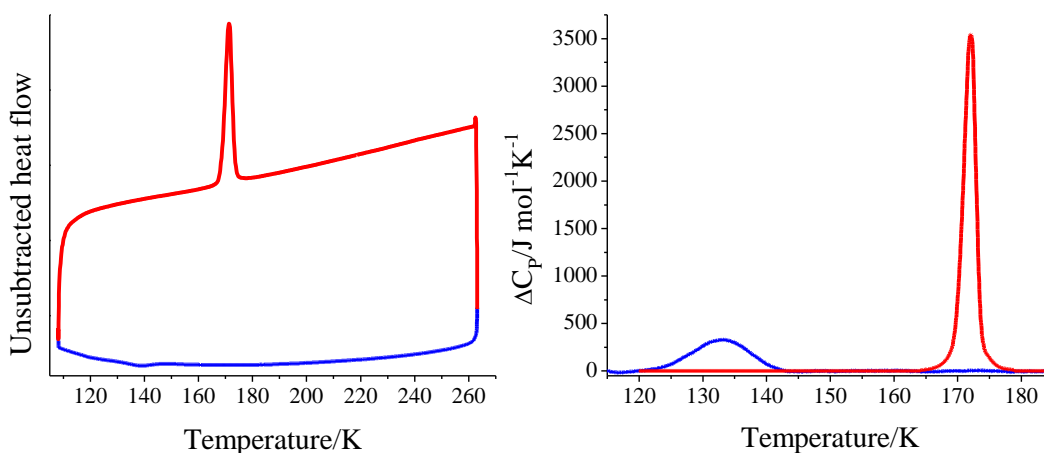
Figure 4.7: (left) The unsubtracted heat flow measured on performing a thermal cycle of compound **1**, with the cooling mode in blue and the heating mode in red. (right) The excess heat capacity, ΔC_P, yielded by the heat flow experiments.

4.5 Magnetic properties (II): Thermally Induced Excited Spin State Trapping

The observation of this memory effect,[13, 14] which causes the spin state of the system to depend on the thermal history of the sample, is indicative of high cooperativity which can

allow for the thermal trapping of a meta-stable HS state.[15] In these rapid cooling experiments, the SQUID cavity is pre-cooled to 10 K, while the sample is maintained at room temperature, in the HS state.[16] The sample holder is then inserted as quickly as possible into the magnetometer, typically taking 10 to 15 seconds, causing the sample to be cooled swiftly to 10 K. This yielded an initial value of χT of 2.42 cm^{3}mol^{-1}K at 10 K (Figure 4.8). Heating the sample at 1 Kmin^{-1} brought about an increase in the value of χT to 3.07 cm^{3}mol^{-1}K at 50 K, due to zero field splitting effects. Therefore, the sample had been fully trapped in a meta-stable HS state. In this low temperature region, the only mechanism which allows relaxation to the LS state involves a process of quantum tunnelling sufficiently slow that the system remains in the HS state while the temperature is raised.[15, 17] At 98 K, the magnetic response of the sample begins to decline sharply, as the system is within the thermally-activated relaxation regime, and the compound gains sufficient thermal energy to rearrange and undergo the transition to the LS state. The stability of this meta-stable state is characterised by a temperature, T(TIESST), defined by the minimum of the derivative of the χT curve with respect to T,[18] which in this case is 106 K. Above 110 K, **1** has fully relaxed to the LS state, and remains diamagnetic until 170 K, where it displays the same behaviour as observed for the thermal cycle, and undergoes an abrupt LS→HS transition with the same value for $T_{1/2}(\uparrow)$. Once at 190 K, the sample was cooled again at 1 Kmin^{-1}, and the effect of the trapping experiment on the hysteresis curve was observed: the thermal hysteresis is now narrower and more symmetric in nature, measuring ~30 K in width.

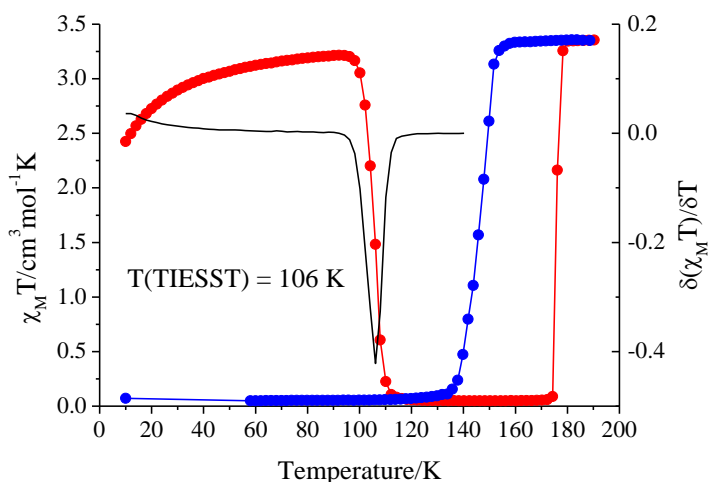**Figure 4.8**: χT vs. *T* curve obtained from the thermal trapping experiment performed on **1** at 10 K. The sample was then heated (red) and subsequently cooled (blue). The inset shows the first derivative of χT with respect to *T*, from which the value of T(TIESST) is derived.

The activation energy, E_a,[17] associated with the relaxation of this meta-stable state to the ground state can be calculated by performing isothermal kinetic experiments and deriving an Arrhenius plot relating the relaxation rate for each curve, k_{HL} with the temperature T. The sample is rapidly cooled to 10 K to induce the full trapping of the meta-stable state, before being warmed to a series of temperatures below that of the thermal spin transition, and the temporal evolution of the magnetic response measured. This permits observation of the time necessary for the meta-stable HS centres to convert to the LS ground state, and the shape of the kinetic curve is intimately related to the level of cooperativity inherent to the system. The relaxation of the thermally trapped meta-stable HS state of **1** is plotted in Figure 4.9 as the normalised HS fraction γ_{HS} against time. As expected, on lowering the temperature at which the relaxation is monitored, the time taken for the compound to relax to the LS state increases. As an initial approximation, the curves were adjusted following an exponential decay model as given by Equations 1.8 and 1.9 in the Introduction. This yielded k_{HL} for each curve, which was then used for the Arrhenius plot in Figure 4.9. As is evident in Figure 4.9, the simple exponential model is an acceptable approach at high temperature, but deviates considerably from the experimental curves at lower temperatures. In fact, the reason for this would prove to be related to the crystal structure of the thermally trapped phase, and is discussed in Chapter 5. However, this method yields $k_\infty = 35066$ s^{-1}, and an associated activation energy E_a of 1129 cm^{-1}.
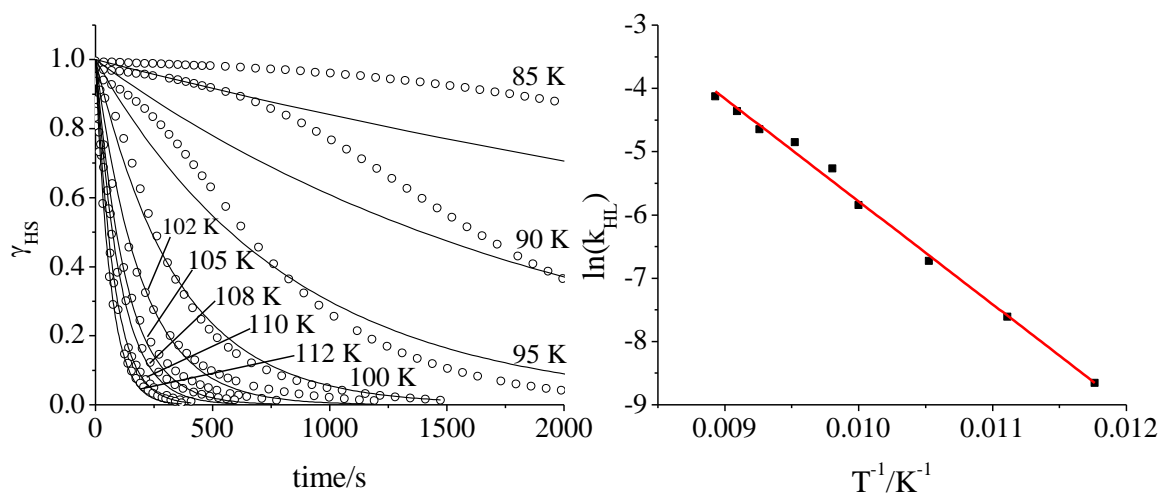

Figure 4.9: (left) Isothermal kinetics experiments of the thermally trapped meta-stable HS state at a series of temperatures, represented as the high spin fraction γ_{HS} *vs*. time. (right) A plot of the characteristic time $\ln(k_{HL})$ *vs*. the inverse temperature. The solid line corresponds to the fit used to extract the kinetic values.

This thermal trapping experiment represents one of the highest values of T(TIESST) obtained for a molecular SCO compound,[19] and is consistent with the inverse energy-gap law.[20, 21] According to this law, the stronger the ligand field experienced by the Fe(II) centre, the larger the zero-point energy gap $\Delta E°_{HL}$ between the lowest vibrational levels of the meta-stable $^5T_2$ HS and ground $^1A_1$ LS states, and so the shorter the lifetime of the meta-stable HS state. This means that high values of $T_{1/2}(\downarrow)$ are associated with low values of T(TIESST), and vice-versa. The combination of this meta-stable HS state, and the broad hysteresis loop observed on performing a thermal cycle in the SQUID magnetometer, allowed further crystallographic experiments to be devised.

4.6 Single crystal X-ray diffraction study (II): Thermally trapped structure, and hysteresis of the unit cell parameters

The range of bi-stability displayed by **1** made a more in-depth crystallographic study feasible, with the aim of understanding the asymmetric nature of the thermal transition from a structural point of view. As such, the thermal sequence to which **1** was subjected in the SQUID magnetometer could be reproduced in a single crystal X-ray diffractometer. The effect on the unit cell angles of **1** as the temperature is lowered and then raised is shown in Figure 4.10, as the given cell angle *vs.* temperature. For all three angles in the triclinic P$_{-1}$ crystal system, the temperature cycle produces a divergence of the parameters depending on the thermal history of the sample, leading to hysteresis loops associated with the unit cell angles. In the cooling mode below 190 K, the parameters α and γ are to be found consistently at lower angles than those observed in the heating mode, until the fully LS state is formed below ~120 K. For the angle β, the cooling mode displays higher values than those of the heating mode, converging above 160 K, and at 85 K. This behaviour is consistent with both the hysteretic nature of the SCO, and the fact that the values of α and γ are higher in the LS state than in the HS state, while the value of β is lower in the LS state.

In addition to the evaluation of the unit cell angles on performing this cycle, full structure determinations were carried out at 150 K on decreasing the temperature, corresponding to the HS state within the hysteresis loop, and the temperature cooled down to 90 K and raised back to 150 K, giving access to the LS state within the hysteresis loop. This sequence of experiments was afforded by the width of the hysteresis cycle in **1**, and the resolution of both spin states at a unique temperature allows the direct effects of
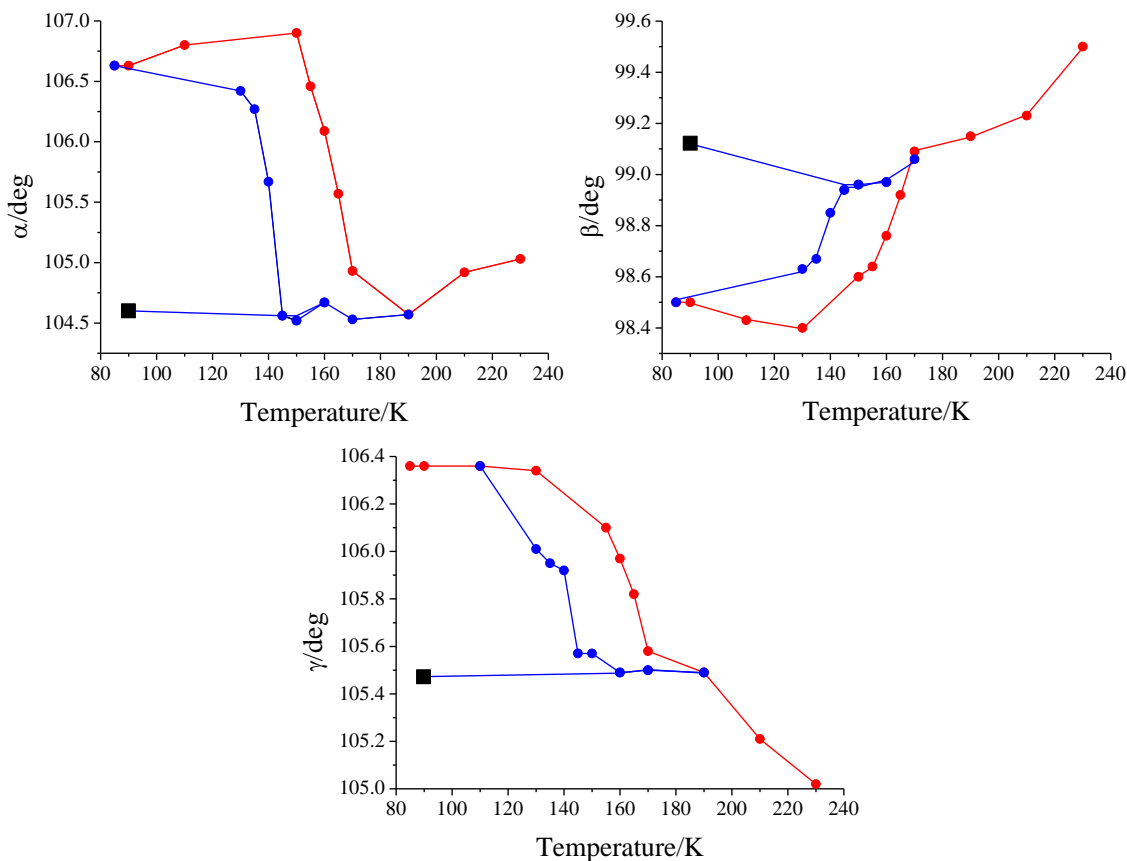
Figure 4.10: Variation of the unit cell angles of **1** on performing a thermal cycle, as determined by single crystal X-ray diffraction. The heating mode is shown in red, with the cooling mode in blue. The black square represents the angle observed on performing a flash cooling experiment.

SCO on a lattice to be observed, irrespective of thermal effects. To this end, a further experiment was performed, involving the flash cooling[16] of a crystal to replicate the thermal trapping experiment of the SQUID. Here, however, the temperature of the diffractometer was lowered to 100 K, and the crystal, pre-mounted on the goniometer, was positioned for collection as quickly as possible, leading to a faster cooling process than that possible for the magnetometer. Comparison of the unit cell dimensions for the structures elucidated at 150 K, shows that the SCO process is associated with their anisotropic modification,[22] with values of $\Delta a = +0.089$ Å, $\Delta b = +0.16$ Å, $\Delta c = -0.074$ Å, $\Delta \alpha = +2.08°$, $\Delta \beta = -0.72°$ and $\Delta \gamma = +0.87°$. These variations of the cell parameters yield a change in the unit cell volume, denoted ΔV_{SCO}, of 0.41 % with respect to the high temperature structure. A more significant change in volume is observed in the coordination octahedron around the Fe(II) centre, which measures 12.43 $Å^3$ at 150 K in the HS state, and 9.77 $Å^3$ in the LS state, a reduction of 21 %. Beyond the cation and unit cell, the nature of the crystal packing and the intermolecular interactions correspond to

those observed for the high temperature HS state and low temperature LS state, with slight variations in the exact strength due to the difference in temperature.

The most important difference noted between the two spin states concerns the level of disorder in the lattice. The high temperature HS state (**A**), the HS state found within the bi-stable domain (**C**), and the thermally trapped meta-stable HS state (**E**) are all seen to

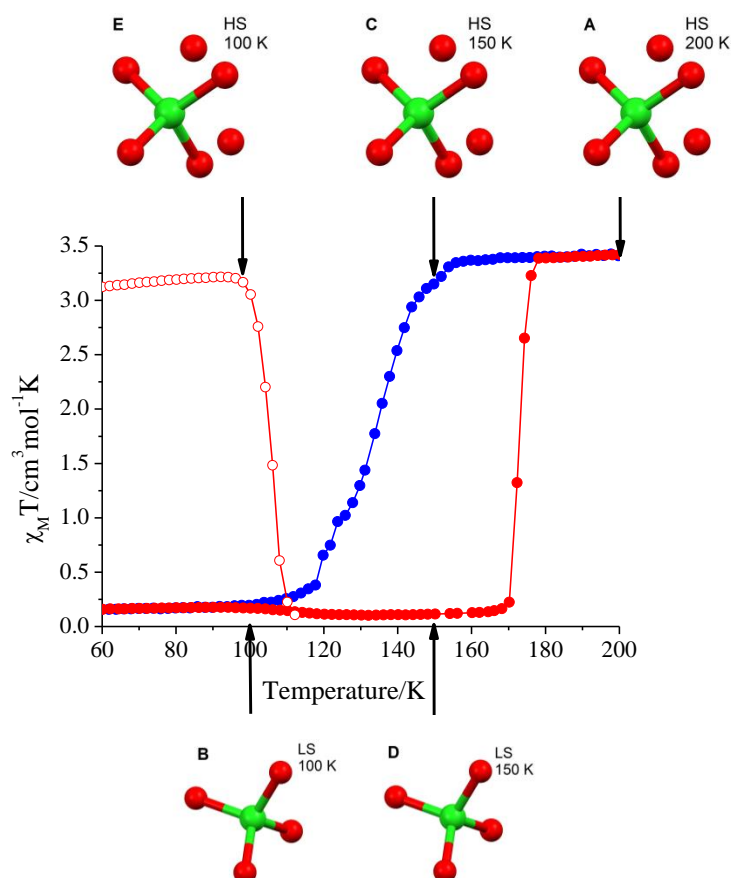| T/K	200 (HS)	150 (HS)	150 (LS)	100 (LS)	100 (HS)
ClO_4^- occupancy (O5,O8:O55,O88)	0.8:0.2	0.8:0.2	1:0	1:0	0.8:0.2
Acetone 1 occupancy (C2S:C3S)	0.4:0.6	0.4:0.6	1:0	1:0	0.4:0.6
Acetone 2 occupancy (C7S:C8S)	0.3:0.7	0.3:0.7	1:0	1:0	0.3:0.7

Figure 4.11 and Table 4.5 : Correlation between the spin state, as derived from the χT value, and the disorder displayed by the system, represented here by one of the perchlorate anions. The occupancies of the disordered entities with various temperatures and in the high and low spin states are given in the table above.

display disorder in both of the acetone molecules and in one of the two perchlorate anions found in the lattice. The nature of the disorder appears to be independent of the temperature, because at all three temperatures, which span a range of 100 K, it is manifested as the same level of split occupancy for the three disordered entities. The spin transition to the LS state at 100 K is accompanied by an ordering of these lattice entities, which then fully occupy one position in the crystal network. The sample was heated to 150 K, placing the system within the hysteresis loop while remaining in the LS state. This structure also presented the full ordering of the spin-inactive components, showing that this ordering is independent of the temperature of the sample. This situation is summarised in Figure 4.11. The combination of these results demonstrates experimentally that the disorder is linked to the spin state of the Fe(II) ion, and that the order/disorder crystallographic transition is coupled to the spin crossover. This leads to a fundamental difference in the processes which occur on cooling or heating: while the cooling mode that induces the HS→LS switch is accompanied by the ordering of lattice entities, the heating mode involves a fully ordered phase. It is proposed that this difference is at the root of the asymmetry observed in the hysteresis loop, with the abrupt transition seen in the heating mode a direct consequence of the ordered state from which the LS→HS transition must occur.

The relaxation of the thermally trapped meta-stable of **1** could be monitored through single crystal X-ray diffraction. In these experiments, the sample was flash cooled to a temperature below that of T(TIESST), and evolution of the unit cell angles measured. The α parameter is the most illustrative, being that which displays the largest difference on undergoing SCO ($\Delta\alpha_{SCO} = +2.06°$), and its temporal evolution is presented in Figure 4.12. At 102 K, the relaxation is observed to begin instantly, reaching the LS state within five minutes. For the measurements at lower temperatures, 97 and 93 K, the process slows, to the extent that for the latter kinetics experiment, there is an appreciable induction period of nearly 500 s, before the HS centres begin to relax. Comparison with the SQUID kinetics experiments at 90 and 95 K, represented here as the normalised low spin fraction γ_{LS} *vs*. time, shows the process as measured for a large polycrystalline aggregate to be similar to that for the monocrystal, and the coupling that exists between structural and magnetic properties.
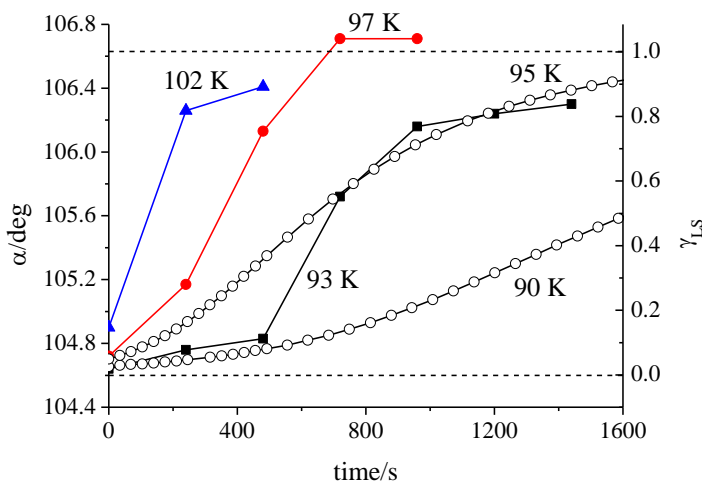
Figure 4.12: Isothermal relaxation of the unit cell parameter α (in blue triangles, red circles, and black squares). The white circles correspond to the SQUID relaxation measurements, characterised by the LS fraction γ_{LS}.

4.7 Magnetic properties (III): Thermal relaxation within the hysteresis loop

The peculiar, asymmetric nature of the spin transition in the cooling mode could be investigated by performing isothermal experiments to follow the temporal evolution of χT at various stationary points within the bi-stable regime. The temperature of the polycrystalline sample of **1** was lowered at 1 Kmin^{-1} to a series of temperatures (160, 156, 150, and 143 K) and the temperature variation stopped. The change in χT with time was then measured as the sample relaxed towards a saturation limit (Figure 4.13). In the case of the experiment at 150 K, the initial χT value is 2.24 cm^{3}mol^{-1}K, and this value decreases to 1.51 cm^{3}mol^{-1}K after two and a half hours. Once this relaxation appeared to have slowed sufficiently, the sample was cooled to the fully LS state at 100 K, before being heated back to the fully HS state at 190 K in preparation for the next experiment. With the exception of the experiment at 160 K, which shows no appreciable relaxation, the shapes of these curves can be described as stretched exponentials, associated with self-decelerating behaviour.[23] Principally, this is caused by differences in the relaxation rates between the different meta-stable states, interpreted as a Gaussian distribution of the energy barriers to relaxation.[24] This leads to a mixture of what would be the exponential curve for each Fe(II) centre, and results in a stretched exponential decline. For **1**, this is especially likely because, as well as the HS$\rightarrow$LS relaxation, there is a simultaneous partial ordering of the spin-inactive components in the lattice.[25] These relaxation processes therefore take longer when compared to the time taken by the thermally trapped

meta-stable HS state described in Section 4.5. The extrapolation of the curves to t_∞ yielded the corresponding final value of χT, which for the case of $T = 150$ K was $\chi T = 1.27$ cm^{3}mol^{-1}K. Using the values derived for all four experiments, a quasi-static hysteresis loop could be traced,[26] which is shown to be well-separated from the initial cooling branch of the thermal cycle. This bi-stable regime is therefore less extensive than that originally measured, with $\Delta T_{1/2} = 25$ K.
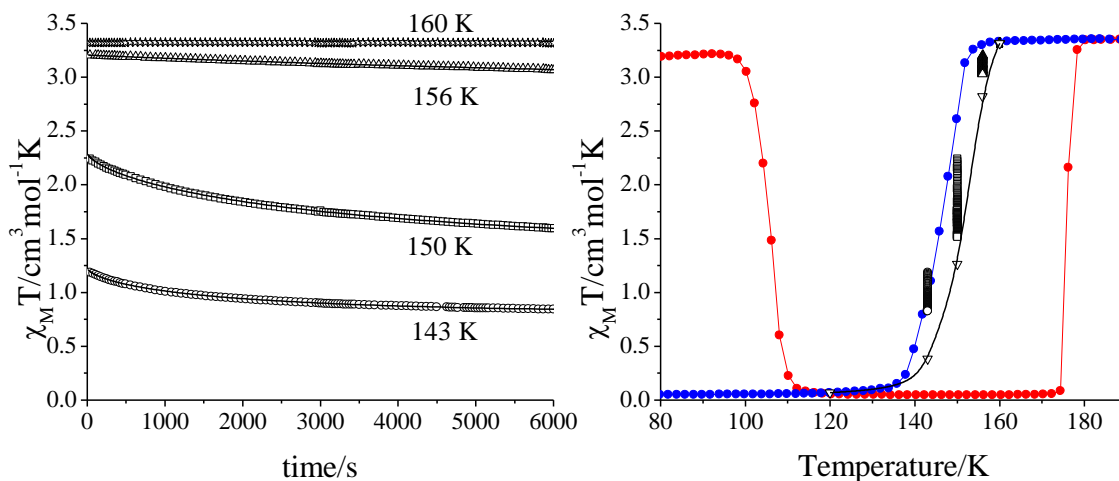

Figure 4.13: (left) Isothermal relaxation experiments of **1** in the region of the hysteresis loop. (right) A representation of this relaxation as χT *vs*. *T*. The white triangles correspond to the extrapolation of the kinetic to t_∞, and the solid black line is the fit corresponding to the "real" hysteresis.

4.8 Single crystal X-ray diffraction study (III): Thermal relaxation within the bi-stable regime.

The accessability of this meta-stable state in the SQUID led to the analogous isothermal relaxation experiment monitored through X-ray crystallography. This was measured as the change in the unit cell angles against time at 135 K, as presented in Figure 4.14. For **1**, the LS presents more obtuse angles α and γ than the HS state, reflected by the increase in these parameters with the passage of time. Conversely, the angle β is smaller in the LS state, leading to the decrease in time of this cell parameter. The conversion of β and γ into the LS values appears to be faster than that of α, which takes more than 30 minutes to reach a value close to the LS state.
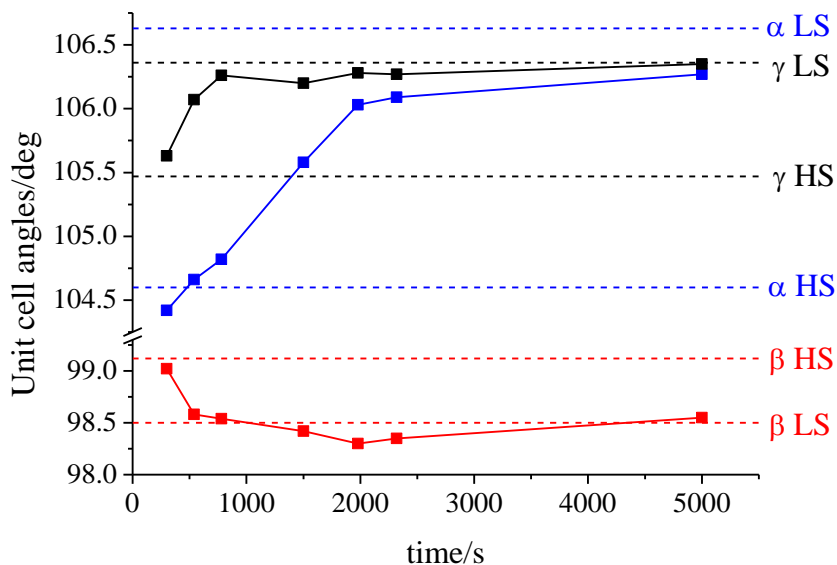
Figure 4.14: Relaxation of the unit cell angles *α* (blue), *β* (red), and *γ* (black) of **1** at 135 K.

4.9 Concluding remarks

The ligand H_4L was successfully employed in the synthesis of a mononuclear Fe(II) complex, with the extended nature of the aromatic molecule leading to an array of intermolecular interactions in the crystal structure. The form of the ligand leads to a particular shape of the cations, which in turn favours a crystal packing arrangement similar to the "terpyridine embrace". The extent of these supramolecular contacts induces a sufficient level of cooperativity in the system for spin crossover to be observed, with an asymmetric bi-stable region in which the spin state of the compound depends on its thermal history. Rapid cooling of **1** induces the thermal trapping of a meta-stable HS state, shown to be stable up to 106 K, which ranks amongst the highest values of *T*(TIESST) observed for trichelate complexes. The elucidation of the crystal structures associated with the HS states at high temperature, within the hysteresis loop and after thermal trapping, together with the LS counter-parts, demonstrated that the thermal SCO is accompanied by a disorder/order transition of the spin-inactive entities in the lattice. This phenomenon is proposed as the cause of the asymmetry observed in the hysteresis loop: the order→disorder transition in the heating mode is manifested as a more abrupt magnetic response than that of the inverse process. There is also a kinetic effect present in the cooling mode, such that isothermal relaxation experiments were used to demonstrate that there is a region of meta-stability within the hysteresis loop. This was proved by the decrease of χT at constant temperature over time as a fraction metal centres relax from the meta-stable phase. A series of measurements in the SQUID were thus used to show the

existence of this meta-stable region, the effect of which is to widen the apparent bi-stable regime of the system. The replication of these isothermal experiments as well as the thermal cycling, for a single crystal, shows the intimate relationship that exists between the spin state of a system and its structural properties.

4.10 References

1. P. Gütlich, A. Hauser and H. Spiering, *Angew. Chem. Int. Ed.*, 1994, **33**, 2024-2054.
2. J. M. Holland, J. A. McAllister, C. A. Kilner, M. Thornton-Pett, A. J. Bridgeman and M. A. Halcrow, *J. Chem. Soc. Dalton Trans.*, 2002, 548-554.
3. J. K. McCusker, A. L. Rheingold and D. N. Hendrickson, *Inorg. Chem.*, 1996, **35**, 2100-2112.
4. M. G. B. Drew, C. J. Harding, V. McKee, G. G. Morgan and J. Nelson, *J. Chem. Soc., Chem. Commun.*, 1995, 1035-1038.
5. J. McMurtrie and I. Dance, *CrystEngComm*, 2005, **7**, 216-229.
6. M. L. Scudder, H. A. Goodwin and I. G. Dance, *New J. Chem.*, 1999, **23**, 695-705.
7. A. L. Spek, *J. App. Cryst.*, 2003, **36**, 7-13.
8. S. A. Barrett, C. A. Kilner and M. A. Halcrow, *Dalton Trans.*, 2011, 12021-12024.
9. O. Kahn, *Molecular Magnetism, Wiley VCH*, 1993.
10. M. A. Halcrow, *Chem. Soc. Rev.*, 2008, **37**, 278-289.
11. S. Bonnet, G. Molnár, J. S. Costa, M. A. Siegler, A. L. Spek, A. Bousseksou, W. T. Fu, P. Gamez and J. Reedijk, *Chem. Mat.*, 2009, **21**, 1123-1136.
12. M. Sorai, M. Nakano and Y. Miyazaki, *Chem. Rev.*, 2006, **106**, 976-1031.
13. O. Kahn and C. J. Martinez, *Science*, 1998, **279**, 44-48.
14. O. Kahn, J. Krober and C. Jay, *Adv. Mat.*, 1992, **4**, 718-728.
15. T. Buchen, P. Gütlich, K. H. Sugiyarto and H. A. Goodwin, *Chem.-Eur J.*, 1996, **2**, 1134-1138.
16. M. Marchivie, P. Guionneau, J. F. Létard, D. Chasseau and J. A. K. Howard, *J. Phys. Chem. Solids*, 2004, **65**, 17-23.
17. A. Hauser, *Top. Curr. Chem.*, 2004, **234**, 155-198.
18. J. F. Létard, *J. Mater. Chem.*, 2006, **16**, 2550-2559.
19. V. A. Money, C. Carbonera, J. Elhaik, M. A. Halcrow, J. A. K. Howard and J. F. Létard, *Chem.-Eur. J.*, 2007, **13**, 5503-5514.
20. A. Hauser, A. Vef and P. Adler, *J. Chem. Phys.*, 1991, **95**, 8710-8717.
21. A. Hauser, *Coord. Chem. Rev.*, 1991, **111**, 275-290.
22. P. Guionneau, M. Marchivie, G. Bravic, J.-F. Létard and D. Chasseau, *Top. Curr. Chem.*, 2004, **234**, 97-128.
23. C. Enachescu, J. Linares, F. Varret, K. Boukheddaden, E. Codjovi, S. G. Salunke and R. Mukherjee, *Inorg. Chem.*, 2004, **43**, 4880-4888.
24. G. Dupouy, S. Triki, M. Marchivie, N. Cosquer, C. J. Gómez-Garcia, S. Pillet, E. E. Bendeif, C. Lecomte, S. Asthana and J. F. Létard, *Inorg. Chem.*, 2010, **49**, 9358-9368.
25. V. Mishra, R. Mukherjee, J. Linares, C. Balde, C. Desplanches, J. F. Létard, E. Collet, L. Toupet, M. Castro and F. Varret, *Inorg. Chem.*, 2008, **47**, 7577-7587.
26. J. F. Létard, S. Asthana, H. J. Shepherd, P. Guionneau, A. E. Goeta, N. Suemura, R. Ishikawa and S. Kaizaki, *Chem.-Eur. J.*, 2012, **18**, 5924-5934.